New Phase in Fluid Hydrogen at Room Temperature

Atsuko Nakayama (atsuko@iwate-u.ac.jp)
Iwate University
Yuya Isurugi
Niigata University
Yuya Serizawa
Iwate University
Satoshi Nakano
National Institute for Materials Science
Ayako Ohmura
Niigata University
Fumihiro Ishikawa
Niigata University

Research Article

Keywords: fluid hydrogen, room temperature, megapascal (MPa), x-ray, nano-space of graphite, gigapascal

Posted Date: July 9th, 2021

DOI: https://doi.org/10.21203/rs.3.rs-671670/v1

Abstract

The presence of phase-transition in hydrogen (H_2) at around 560 megapascal (MPa) and room temperature was clarified by Raman and x-ray diffraction studies on both pure H_2 and graphite-H_2 mixture. H_2 is intercalated into the nano-space of graphite, which lowers the transition pressure and temporally expands the size of the honeycomb lattice of graphite under pressure up to 600 MPa. It is supposed that is caused by a gas-liquid phase-transition. According to the peak analysis for $Q_1(J)$ mode, the ortho-para conversion of H_2 gradually begins to appear after the phase-transition pressure even at room temperature, while peak separation is difficult to achieve under pressure above 1.6 gigapascal (GPa) because of significant overlapping of the peak intensities. Because we have missed the ortho-para conversion which could be observed in only such a small pressure range, the fluid phase at room temperature was full of mystery.

Introduction

Many researchers have clarified the detailed-phase diagram of hydrogen (H_2), particularly, solid H_2 in a multi-megabar pressure-range in order to explore the metallic phase [1–4]. On the other hand, it is necessary for us to know the information on the physical properties of fluid H_2 in order to use H_2 effectively and safely in the future of clean energy. We have some information on the fluid state at room temperature[5–7] in the current phase diagram, though the phase boundary between the fluid and solid is known to be 5.4 GPa at room temperature[8]. Previously, it has been considered that the phase boundary between gas and liquid of H_2 was difficult to observe at room temperature. The results of simultaneous measurements of molar volume and ultrasonic velocity of fluid H_2 gave a single equation of state up to 20 kbar at room temperature[6]. According to the recent studies on supercritical fluid phase of H_2 by Raman spectroscopy and x-ray diffraction, however, a peculiar behavior was observed at the pressure 1 ~ 2 GPa at room temperature[9]. It was analyzed to be affected by enhancement of the intermolecular interaction based on the phase transition to the liquid or solid. This is important information which cannot be overlooked in developing hydrogen-storage materials. Another important thing to understand about the properties of H_2 is to comprehend the effects of H_2 on its surroundings. For example, hydrogenation of various metals[10–12], and their metal hydrides[13–15] have been studied even under high pressure. High pressure accelerates hydrogenation, which can lead to results in a short time. On the other hand, the detailed phenomena generating in H_2 molecules in the mega-pascal pressure range, is overlooked, because many researchers pay too much attention on the metallization of H_2[1–4,16]. As a matter of course, there should be also consequences of significant and interesting changes in such a low-pressure range.

In our previous study, multi-walled carbon-nanotubes whose tips were removed (the opened-MWCNTs), were compressed with H_2 gas in DAC at room temperature[17]. *In situ* x-ray diffraction (XRD) clarified that the C—C bond of six-membered ring on MWCNTs expands by 0.27% at 0.57 GPa in spite of large Young's modulus on the order of 1.0 TPa[18]. The interlayer distance, however, monotonously decreased with

pressure. In contrast, the closed-MWCNTs showed monotonous compressions of both the C—C bond and interlayer distance. It suggests that H_2 is intercalated in the opened-MWCNTs, resulting in the generation of some special interaction between the π-electron system of MWCNTs and atomic or molecular H_2 even in the mega-pascal pressure-range. The cylindrical framework of MWCNTs, which were composed by bending the multi-layered graphene-sheets, has a large strain energy; therefore the effect of H_2 under high pressure should also be different from graphite having a two-dimensional (2D) structure[19]. In order to solve a mystery on expanding the C-C bond of MWCNTs compressed together with H_2, we need to understand the properties of pure H_2 under pressure at around 0.5 GPa. Furthermore, in order to clarify our question, it is necessary to investigate the effect from H_2 by using graphite as the host, which has one of the simplest structures among carbon materials. That motivated us to study the physical properties of H_2 and graphite-H_2 mixture in the mega-pascal pressure-range.

Pressure dependence of Raman spectra of supercritical fluid H_2 was investigated in detail under pressure up to 2 GPa at room temperature in this study. We also focused on the properties of H_2 compressed with graphite, which has a planer structure unlike MWCNTs. It was reported that graphite causes the intercalation of H_2 under pressure at least above 10 GPa[19], however, there is no evidence of that under a lower pressure. We expect that graphite works as the probe detecting anomalies of H_2 under pressure if graphite also intercalates H_2 like the opened-MWCNTs. Therefore we measured Raman spectra of graphite-H_2 mixture to obtain the information of C-C bond of graphite and vibration of H_2, which were simultaneously compressed. In addition, *in-situ* structural observation of XRD of graphite-H_2 mixture was also carried out up to 2 GPa at room temperature. It is difficult to measure XRD of fluid H_2, but we were able to extract the information on H_2 from the structural change in graphite which could be affected by H_2.

Methods

Setup of pressure generation device with sample mounted

A diamond anvil cell (DAC) was used to generate the pressure. We prepared two kinds of samples which were mounted in DAC: one was H_2 and the other was the mixture of graphite and H_2, graphite-H_2. For pure H_2, only Raman spectra were measured. In case of graphite-H_2, not only Raman spectra but also XRD images were observed. Type IIa and Ia diamond anvils, were used for both Raman and XRD measurements, respectively; each anvil has 0.8 mm in culet diameters and 2 mm in thicknesses. The metal foil with 200-μm initial-thickness, made of wolfram having hydrogen-proof properties, was used as the gasket material. The indentation was formed on the gasket surface using the pair of diamond anvils; a hole was made at the center of dent on the gasket by electron discharge machining. In this way, the gasket hole with the 300 μm in diameter and 100-μm thickness was prepared as the sample room in DAC. Ruby balls for the pressure marker were put in the hole. The magnitudes of pressures loaded on the

samples were determined from the fluorescence peaks of ruby balls put in the sample chamber on the basis of ruby R_1-line pressure-scale[20].

The sample for the Raman measurements of H_2, were prepared by filling the gasket hole with high-density H_2-gas with 99.999% purity, which was compressed up to 180 MPa at room temperature using a gas loading system in NIMS[21]. In cases of measurements of graphite-H_2, instead of using graphite powder we chose meso-carbon micro-beads (MCMBs) having a specific surface area smaller than 2.0 m^2/g, supplied by Osaka gas Co. Ltd. For powder XRD experiments, fine and smooth Debye-Scherr rings are required for analysis. Graphite has a large linear modulus of elasticity from the *a*-axis direction due to sp^2 hybridized bonding between C atoms, while the van der Waals force between graphene layers dominating the *c*-axis length is very weak. This causes the stacking disorder and lattice distortion of graphite after grinding into fine powder. The grains of MCMBs were lightly beaten in the agate mortar; the submicron sized grains were put in the hole, which was filled with the dense H_2 gas like the former method.

In situ **observations of Raman spectra and XRD.**

An 180º backscattering geometry and excitation wavelength of 514.5 nm provided by an Ar ion laser, were employed for the Raman spectral measurements. The spectra were obtained using a microscopic Raman spectrometer, which had a single monochromator (Jobin Yvon/ ATAGO BUSSAN CO. LTD., T64000), and a liquid nitrogen cooled charge-coupled device (CCD) detector. The laser beam was focused to 4.7 μm spot on the sample, at which the laser power was around 9 mW for the sample with the diamond anvil. The magnitudes of spectral resolutions are 4.76 and 2.82 cm^{-1} at the spectral centers of 620 and 4200 cm^{-1} in case of a 200 μm slit width, respectively. Raman spectra at each pressure was obtained by averaging 3 runs with one scan for 10 min in each run. The pure rotation and vibration-rotation bands of H_2 were measured at the same focal point where G-band was obtained at each pressure. Each substantial spectrum of the sample was obtained by subtracting the spectrum of the gasket through the diamond anvil from the raw spectrum, which were obtained at each pressure. Neon emission line was used to calibrate the wave numbers of the spectra measured.

To understand the influence of H_2 on the structure of graphite under high pressure, in-situ XRD was carried out using synchrotron radiation (SR) beams on BL-18C at Photon Factory, High Energy Accelerator Research Organization (KEK). The x-ray beam monochromatized in 20 keV, was introduced to the specimen through a collimator with 100 μm in a pinhole diameter. Each angle-dispersive powder-patterns was obtained by exposing the x-ray beam to the sample for 15 min at room temperature. An imaging plate as a detector and Typhoon FLA 7000 scanner, supplied by Fuji Photo Film Co. Ltd. and GE Healthcare, respectively, were used to obtain the 2D powder XRD images. One image contains 2000×2560 pixels with a resolution of 100×100 μm^2 per pixel. The 2D XRD image were integrated along the Debye-Scherrer rings with 0.02 degrees of 2θ step.

Results And Discussion

Phase transition of fluid H_2 inducing ortho-para conversion

Raman spectra from pure rotation modes, S_0 (J) (J = 0 to 2), and vibration-rotation modes, Q_1 (J) (J = 0 to 3), of H_2, measured at each pressure, are shown in Fig. 1, where J is the rotational quantum number. The S_0 (3) peak was also measured, however the intensity was very weak, so that was omitted from the analysis. Every S_0 (J) peak showed a decrease in peak height and linewidth expansion with an increase in pressure up to 2.05 GPa. In case of Q_1 (J) modes, only the Q_1 (0) peak disappeared under pressure above 0.68 GPa; further pressurization caused increase of overlap between the Q_1 (J) (J = 1 to 3) peaks, which looks like one peak under pressure above 1.48 GPa.

Line shapes of the S_0 (J) peaks were analyzed using Lorentz functions; pressure dependence of Raman shift is shown in Fig. 2a. All S_0 (J) mode show monotonous changes in Raman shifts except a sharp risie at around 0.5 GPa as shown in an enlarged view of Fig. 2b. To estimate the transition pressure P_c, two tangent lines were drawn on the Raman shift-pressure plots of S_0 (J). The value of P_c is estimated from the position of intersection point between the two lines, which is obtained to be in average 0.56 GPa for the S_0 (J) peaks. The S_0 (J) peaks are the Stokes spectral lines caused by the rotational transition, $J \rightarrow J$ + 2, respectively, as shown in Fig. 2c; the selection rule for the rotational and vibrational quantum numbers has ΔJ = +2 and Δv= 0 in this case[5]. The magnitude of Raman shift for each S_0 (J) mode corresponds to the transition energy. Correlation of the energy levels of J could be changed under pressure above 0.56 GPa. Pressure dependences of full widths at half maximums, FWHMs, of S_0 (J) peaks also show anomalies at around 0.56 GPa, as marked with an arrow in Fig. 2d. In addition to the anomaly observed in the pressure dependence of Raman shift, sharp widening of the linewidth could be caused by pressure-induced phase-transition of H_2. The pressure changes in relative intensities for the S_0 (J) modes normalized using that for S_0 (1) were shown in Fig. 2e. The intensity for the S_0 (0) mode is almost constant under pressure up to 1 GPa but slightly increases with increase the pressure beyond 1 GPa; it means the increase of transition probability, J = 0 to J = 2, in the para-H_2. In contrast that for the S_0 (2) mode is almost constant up to 2.04 GPa.

The Q_1 (J) peaks overlapping in the narrow frequency range, were decomposed using multiple Lorentz functions as shown in Fig. 3a. The vibration-rotation spectrum consists of the Stokes Q_1 (J) lines, which are generated by the vibrational transition, n = 0 → n = 1, and the rotational transition, $J \rightarrow J$, respectively[5], as shown in Fig. 3b. The line-shapes for Q_1 (J) modes drastically change in the pressure range between 0.68 and 1.29 GPa. The Q_1 (0) band disappears at the pressure above 0.68 GPa; the Q_1 (2) band shows the increase of peak intensity. Although the Q_1 (1) band shows a decrease of peak height and an increase of FWHM with an increase in pressure, the Q_1 (3) peak intensity looks constant even though the pressure is increasing.

Figure 3c and d show the pressure dependences of Raman shifts and FWHMs for Q_1 (J) modes of H_2, respectively, which show the rapid increasing at pressure around 0.5 GPa as same as those for S_0 (J) modes. The Raman shifts of Q_1 (J) modes except Q_1 (0) one showed monotonous changes with increasing the pressure above 0.5 GPa. The intensity for Q_1 (0) mode was broaden and disappeared under pressure above 0.68 GPa. The value of P_c on average for Q_1 (J) modes except Q_1 (0) one was estimated at 0.56 GPa, which is the same value for S_0 (J) modes; the data for Q_1 (0) mode were not enough to obtain the value P_c. At pressures above 0.68 GPa, the FWHMs of Q_1 (1) and Q_1 (3) modes increased with increase of pressure. On the other hand, FWHM for Q_1 (2) mode showed constant in the pressure dependence above 1.0 GPa. The pressure changes in relative intensities for the Q_1 (J) modes were normalized where using those Q_1 (1) as shown in Fig. 3e. The intensity for Q_1 (0) mode decreased with an increase in pressure and disappeared at the pressure above P_c. The Q_1 (2) mode showed drastic enhancement of the intensity under pressure above P_c; the intensity for Q_1 (2) mode overtakes that for Q_1 (1) under pressure higher than about 1 GPa. It means that the vibrational-excited state of J = 2 increased with pressure in comparison with that of J = 1, suggesting progression of the pressure-induced ortho-para conversion at room temperature. The ortho-para conversion initially revealed at low temperature[20], has recently been found in catalytic reactions[23] or in high-pressure condition at low temperature[24].

The following interpretation can be considered for the pressure dependence of peak intensities for Q_1 (J) modes. Para-H_2 has an isotropic orientation of nuclear spins in case of J = 0. When H_2 molecules get close to each other through compression, the inter-molecular interaction becomes strong; the molecular rotation is suppressed and causes anisotropy of the orientation. For this reason, the state of J = 0 is mixed with that of J = 2 by pressurization; the increase of intensity of Q_1 (2) occurs in parallel with the decrease of Q_1 (0). If the state of J = 1 for ortho-H_2 are occupied in all directions with equal probability, H_2 molecules do not orient in any special direction. Pressurization generally suppresses the rotational motion, resulting in anisotropy for ortho-H_2, as well as the case of para-H_2. Since the state of J = 3 is mixed into that of J = 1, depressing of the Q_1 (1) peak intensity should be accompanied with enhancement of the Q_1 (3) peak intensity. Contrary to such assumptions, in fact, the intensity of Q_1 (3) did not increase significantly though diminishing that of Q_1 (1); only Q_1 (2) mode showed drastic increases of intensity. Therefore, it is speculated that the pressurization beyond 0.56 GPa accelerates ortho-para conversion of H_2 even at room temperature.

Fluid H_2 causing anomaly of graphite structure under megapascal-class pressure

We also carried out the Raman measurements of H_2 pressurized with graphite, which were compared with those of pure H_2 in order to confirm the reproducibility of transition which was found in pure H_2 and to explore the possibility of intercalation of H_2 into graphite. In addition to the spectra for S_0 (J) (J = 0 to 2) and Q_1 (J) (J = 0 to 3) modes of H_2, G-band from graphite are also shown in Fig. 4. The signal to noise

(SN) ratio of G band became low at pressure around 0.15 GPa as shown in Fig. 4a, which was improved by further pressurization. It is considered that the SN ratio temporarily deteriorated at low pressure due to the change in the reflectance at the interface between diamond and compressed H_2. All the S_0 (J) modes except S_0 (2) modes, and Q_1 (J) modes showed the minimums in the intensities at the pressure around 0.47 GPa as shown in Fig. 4b and c, respectively. In order to check the reproducibility of such strange behaviors, the Raman spectra of 0.47 GPa were measured again after an interval of several hours. All peak positions obtained in the second observation shifted slightly in comparison with those of the first observation. The intensities particularly for S_0 (J) and Q_1 (J) modes drastically increased in the second observation of 0.47 GPa. In this way pressurization at around 0.5 GPa caused the instability of vibrations. On the other hand, under the pressure more than 0.6 GPa, the S_0 (2) mode which was once difficult to observe under pressure above 0.33 GPa, was revived again; after that their linewidths and intensities increased when increasing the pressure. The intensity of G-band also grew at a pressure higher than 0.68 GPa. Overlapping of the linewidths for Q_1 (J) modes proceeded with an increase in pressure, while the intensity of Q_1 (0) mode flattened and expanded with increasing pressure, which was difficult to analyze under pressure above 0.68 GPa. This means that such a series of drastic variations in the spectral intensities is caused by a major change in the reflectivity at the interface between the upper diamond anvil and H_2. It can be considered that an alternation in the reflective index of H_2 was brought by something like a phase transition or change of state in H_2.

The line-shapes of G-band, the S_0 (J) and Q_1 (J) peaks, respectively, were analyzed using Lorentz functions; the pressure dependence of each Raman shift is shown in Fig. 5. The values of Raman shift of G-band which were observed at around 0.5 GPa, caused fluctuation of wave numbers in the range between 1583 and 1586 cm^{-1} as shown in Fig. 5a. The magnitude of FWHM for the G-band also showed fluctuation at around 0.5 GPa, after that expanded with increasing pressure as shown in Fig. 5b except for the range from 0.9 to 1.3 GPa. Such a significant increase of FWHM of the G-band under pressure beyond around 0.5 GPa suggests a shortening of phonon-relaxation time for graphite due to scattering by the densified H_2[25,26] which may be accommodated in the interlayer space of graphite. Because the molecular size of H_2 is smaller than the interlayer distance or the diagonal length of benzene ring composing the honeycomb lattice, H_2 may be accommodated and densified in the nano space of graphite. In short, it means that the densified H_2 changes the phonon-lattice relaxation mechanism of graphite. We suppose that the change observed at around 0.5 GPa is one of the proofs of intercalation of H_2 into graphite.

The pressure dependences of Raman shift and FWHM for the S_0 (J) and Q_1(J) modes of H_2, which were obtained in graphite-H_2 mixture, are expressed in Fig. 5c to f. The S_0 (J) and Q_1 (J) modes also caused flip-flop of the Raman frequencies and FWHMs at the pressure where the fluctuations were observed in the G-band. Although the variation in the pressure dependence observed in graphite-H_2 mixture is larger than that for pure H_2, both this flapped variation of data in common. We were also concerned that only the S_0 (0) mode in graphite-H_2 causes large dispersion of the Raman shift under pressure above 1.6 GPa,

which was not emerged in pure H_2. As a result of the peak decomposition, the pressure changes in Q_1 (J) peak intensities for H_2 in graphite-H_2 mixture were almost same as those of pure H_2 in Fig. 3a. Although the magnitudes of linewidths for Q_1 (1) and Q_1 (3) modes increased with an increasing of the pressure, the that of Q_1 (2) showed constant not only pure H_2 but also in the graphite-H_2 mixture.

We suppose that such a series of abnormal behaviors following the flip-flops are probably caused by a phase transition in H_2: a liquid phase is one of the candidates for the post-phases at room temperature, which has been previously unreported. We need further verification through alternate investigation and experiment. The values of P_c estimated using the pressure changes in Raman shift for the S_0 (J) and Q_1 (J) modes of pure H_2 and graphite-H_2 mixture, are summarized in Table 1. The values of P_c estimated using the results for the S_0 (J) and Q_1 (J) modes obtained in graphite-H_2 were calculated to be 0.46 and 0.48 GPa in average, respectively; the difference is slightly 0.02 GPa, which is within the margin of error. In any case, the magnitude of P_c on H_2 obtained in graphite-H_2 mixture is smaller than that in pure H_2. It means that graphite plays a role of reducing the magnitude of P_c of H_2. Therefore, it is speculated that graphite suppresses the vibration of H_2 through accommodation of H_2 in the interlayer space of graphite or adsorbed on the surface even at room temperature.

According to the high-resolution transmission-electron microscope (TEM) image as shown in Fig. 6a, it was confirmed that the inner part of each grain before pressurization showed a well-stacked graphite-structure with almost all the same spacing between graphene layers. All the XRD experiments gave Debye-Scherrer rings, which have sufficient quality to do the structural analysis as shown in Fig. 6b. The uniformed diffraction ring evidenced the appearance of an unknown peak, which is shown in Fig. 6b, was also confirmed at each pressure, though it was never observed in the pristine sample. The 2D XRD-images from which some contaminations were removed, were integrated along the rings with 0.02 degrees of 2q step. The diffraction pattern of graphite obtained at atmospheric pressure, showed the 002, 100, 101, and 004 reflections from hexagonal symmetry with a space group $P6_3/mmc$ as shown in Fig. 6c. Pressurization of the graphite-H_2 mixture caused the unknown reflection at around 16 degrees, which also remained in the sample released from the pressure. Furthermore, the second unknown peak appeared at around 15 degrees only at the pressure of 0.46 GPa. We confirmed these peaks do not come from the metal gasket. No peaks were observed at angles lower than 2q =10 degrees. The lattice parameters, a and c, were obtained by fitting of the peak intensities using Gaussian functions. The values of lattice parameters of 1 atm were determined to be a_0 = 2.4556 ± 0.0004 and c_0 = 6.7053 ± 0.0002 Å, respectively. The pressure dependence of lattice parameters is shown in Fig. 6d. The c-axis length monotonously decreases when intensifying the pressure above 0.16 GPa.

On the other hand, the a-axis length compressed with H_2 continues to be elongated to 0.6 GPa with some degrees of fluctuations. The maximum of a-axis length is longer than the a_0-axis length by 0.27%, which was almost same as that of MWCNTs. Under pressure above 0.6 GPa the a-axis length decreases with an increase of pressure, which does not become shorter than the a_0-axis length even if the pressure is

beyond 2 GPa. We suppose that the change in the *a*-axis length indicating the maximum is generated by H_2 intercalated into the interlayer space of graphite or the nano-space of the honeycomb lattice. The compressibility of H_2 which changes before and after the phase transition, should be reflected on the change in the *a*-axis length. The unknown peak appeared next to the 100 reflection under pressure above 0.11 GPa; the *d*-value was obtained at $d \approx 2.5$, which is about 2% larger than the *a*-axis length. The values of lattice parameters of the sample released from the pressure were basically restored to the initial state. On the other hand, the unknown peak observed at around $d \approx 2.5$, remained after releasing the pressure from the sample. Appearance of the unknown extra peaks by pressurization suggests that H_2 is accommodated in the interlayer space of graphite. We speculate that the alternating stacking rule of graphite was partially broken by filling H_2 into the inter layer space.

Declarations

Acknowledgements

The authors thanks Dr. T. Kikegawa of KEK and S. Taguchi of Niigata Univ. for their help on XRD experiment at BL-18C, Prof. Yuh Yamada of Niigata Univ., Dr. K. Aoki of Tokyo Univ., and Dr. T. Ishikawa of NIMS for informative discussion. This work was performed under the approval of the Photon Factory Program Advisory Committee (Proposal No. 2004G236 and 2010G525). This work was supported by JSPS KAKENHI Grant Number 24550150 and 20045003.

Author Contributions

A. N. preformed the experiments, analyzed and considered the interpretation of results, and wrote the manuscript of the paper. Y. I. performed the experiments and Y. S. analyzed the results. S. N. performed H_2-gas filling-experiment into DAC. A. O. and F. I. contributed in the discussion on results and supported of the XRD experiments as the co-workers of high pressure laboratory.

References

1. A. Goncharov, *Low Temp. Phys.* **46**, 97-103 (2020).
2. R. P. Dias, and I. F. Silvera, *Science* **355**, 715-718 (2017).
3. M. I. Eremets, and A. Troyan, *Nature Materials* **10**, 927-931 (2011).
4. S. T. Weir, A. C. Mitchell, and W. J. Nellis, *Phys. Rev. Lett.* **76**, 1860-1863 (1996).
5. B. P. Stoicheff, *Canadian J. Phys.* **36**, 730-741 (1957).
6. R. L. Mills, D. H. Liebebergm J. C. Bronson, and L. C. Schmidt, *J. Chem. Phys.* **66**, 3076-3084 (1977).
7. N. E. Moulton, G. H. Watson, W. B. Daniels, D. M. Brown, *Phys. Rev.* A**37**, 2475-2481 (1988).

8. S. K. Sharma, H. K. Mao, and P. M. Bell, *Phys. Rev. Lett.* **44**, 886-888 (1980).
9. Y. Akahama, R. Miyamoto, S. Nakano, S. Kawaguchi, N. Hirao, and Y. Ohishi, *Appl., Phys*. **128**, 135901 (2020).
10. A. P. Drozdov, P. P. Kong, V. S. Minkov, S. P. Besedin, M. A. Kuzovnikov, S. Mozaffari, L. Balicas, F. F. Balakirev, D. E. Graf, V. B. Prakapenka, E. Greenberg, D. A. Knyazev, M. Tkacz, and E. I. Eremets, *nature* **569**, 528-531 (2019).
11. H. Liu, I. I. Naumov, R. Hoffmann, N. W. Aschroft, R. J. Hemley, *Proc. Natl Acad. Sci. USA* **114**, 6990-6995 (2017).
12. S. Takagi, Y. Iijima, T Sato, H. Saitoh, K, Ikeda, T. Otomo, K. Miwa, T. Ikeshoji, and S. Orimo, *Sci. Rep*., **7**: 44253 (2017).
13. T. Matsuoka, H. Fujihisa, N. Hirao, Y. Ohishi, T. Mitsui, R. Masuda, M. Seto, Y. Yoda, K. Shimizu, A. Machida, K. Aoki, *Phys. Rev. Lett.* **107**, 025501 (2011).
14. A. Machida, T. Watanuki, D. Kawana, and K. Aoki, *Phys. Rev*. B **83**, 054103 (2011).
15. D. Meng, M. Sakata, K. Shimizu, Y. Iijima, H. Saitoh, T. Sato, S. Takagi, and S. Orimo, *Phys. Rev*. B **99**, 024508 (2019).
16. R. T. Howie, P. D. Simpson, E. Gregoryanz, *Nat. Mater.* **14**, 495-499 (2015).
17. A. Nakayama, S. Numao, S. Nakano, S. Bandow, and S. Iijima, *Diam. Relat. Mater.* **17**, 548-551 (2008).
18. K. T. Kashyap, and R. G. Patil, *Bull. Mater. Sci.* **31**, 185-187 (2008).
19. J. Lim and C. Yoo, *Appl. Phy. Lett*. **109**, 051905 (2016).
20. C. S. Zha, H. K. Mao, and R. J. Hemley, *Proc. Natl. Acad. Sci*., **97**, 13494-13499 (2000).
21. K. Takemura, P. Ch. Sahu, Y. Kunii, and Y. Toma, *Rev. Sci. Instrum*. **72**, 3873-3876 (2001).
22. E. J. Allin, A. H. Mc Kauge, V. Soots, and H. L. Welsh, *J. de Phys.* **26**, 615-620 (1965).
23. T. Kosone, A. Hori, E. Nishibori, Y. Kubota, A. Mishima, M. Ohba, H. Tanaka, K. Kato, J. Kim, J. A. Real, S. Kitagawa, and M. Takata, *R. Soc. Open sci.* **2**, 150006 (2015).
24. J. H. Eggert, E. Karmon, R. J. Hemley, H. Mao, and A. F. Goncharov, *Proc. Natl Acad. Sci. USA* **96**, 12269-12272 (1999).
25. A. Nakayama, K. Suzuki, T. Enoki, C. Ishii, K. Kaneko, M. Endo, and N. Shindo, Solid. State Commun. 93, 323-326 (1995).
26. K. Sugihara, A. Nakayama, and T. Enoki, *J. Phys. Soc. Jpn.* **64**, 2614-2620 (1994).

Tables

Table 1. Transition pressure, P_c, of H_2 derived from Fig. 2a, 3c, 5d and 5e, respectively, according to the definition explained in Fig. 2b. The values of P_c could not be obtained for Q_1 (0) mode, because of the disappearance of the intensities at around the pressure showing anomaly of data.

		Transition pressure, P_c, of H_2 (GPa)	
		Pure H_2	Graphite-H_2
Rotational modes of H_2	S_0 (0)	0.56	0.46
	S_0 (1)	0.56	0.46
	S_0 (2)	0.56	0.46
Vibrational modes of H_2	Q_1 (0)	—	—
	Q_1 (1)	0.56	0.47
	Q_1 (2)	0.56	0.49
	Q_1 (3)	0.56	0.48

Figures

Figure 1

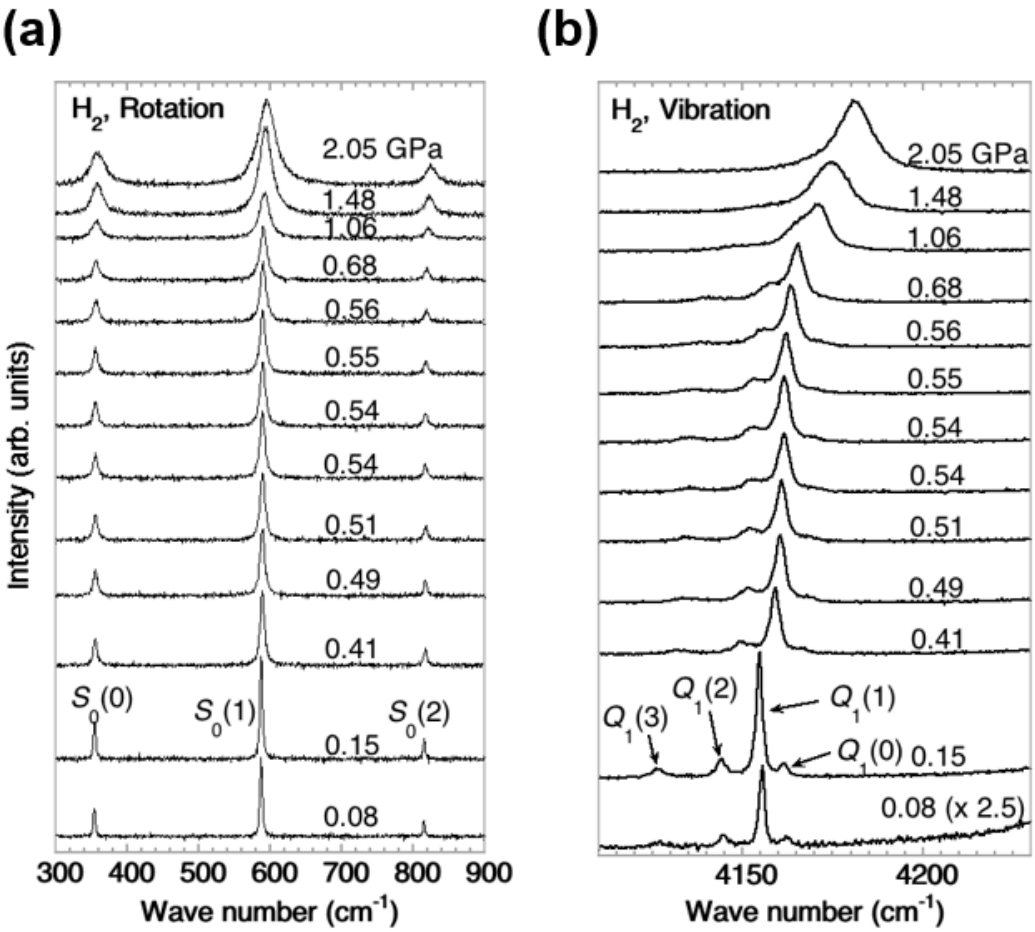

Figure 1

Superimposed display of Raman spectra of H2 under pressure up to 2.05 GPa at room temperature. (a) Rotation modes, S0 (J), (J = 0 to 2). (b) Vibration-rotation modes, Q1 (J), (J = 0 to 3). The S0 (3) band was also observed in this experiment, however the intensity was very weak, so it was omitted in this study. The intensities of Q1 (J) modes observed at 0.08 GPa are very weak, so the Raman spectrum was extended 2.5 times from the original in order to make the spectral structure clear.

Figure 2

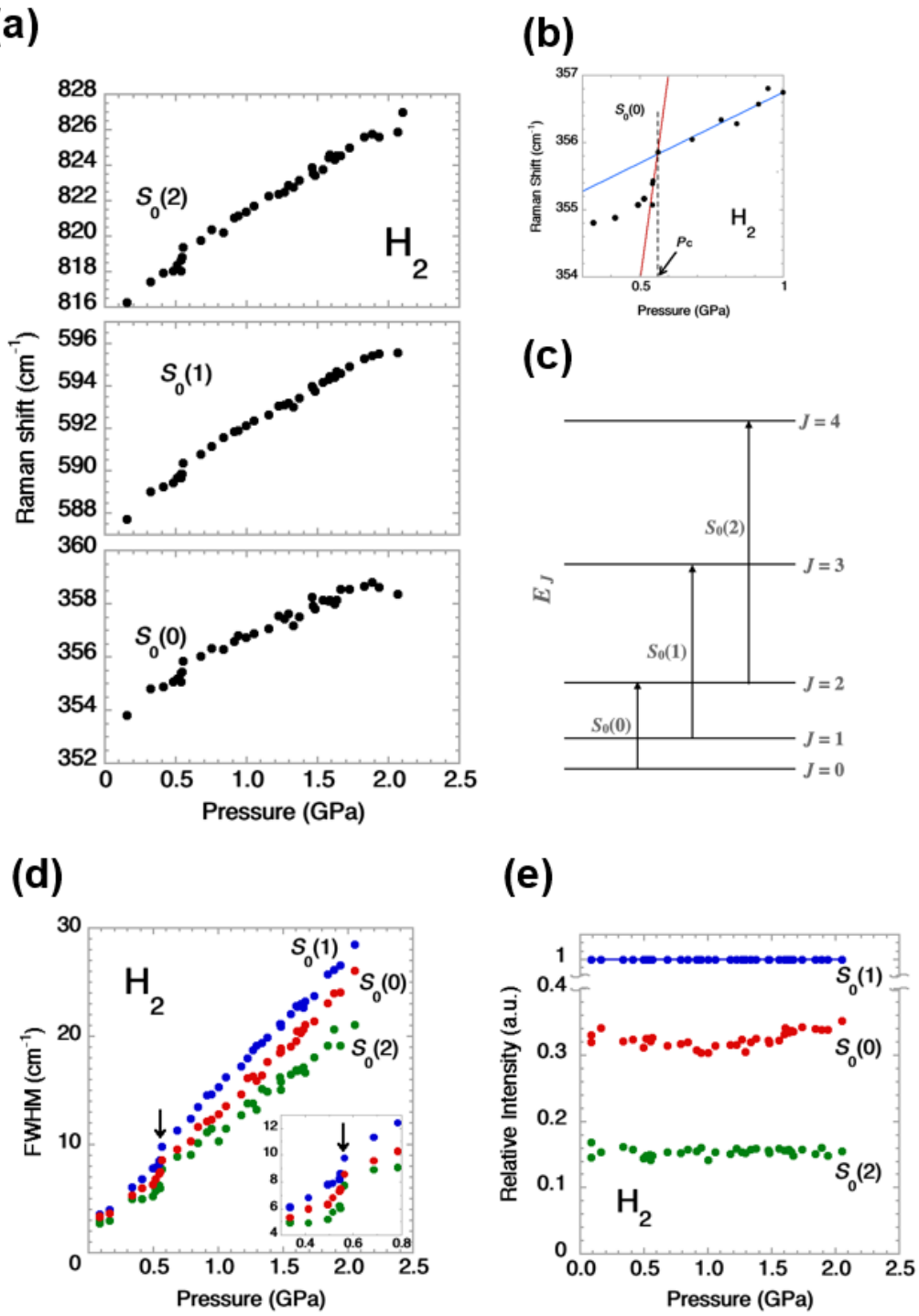

Figure 2

Pressure dependence of Raman shift, FWHM and relative intensity of S0(J) band, obtained from H2. (a) Pressure dependence of Raman shift. (b) Definition of the transition pressure Pc in this study. Two tangent lines of blue and red were drawn in the normal state parts of data before and after the transition. The value of Pc is estimated from the position of the intersection point between the two lines. (c) Scheme of the rotation transitions having the selection rules of $\Delta\upsilon = 0$ and $\Delta J = +2$ on the Stokes line. (d)

Pressure dependences of full widths at half maximums (FWHMs). The insert of shows enlarged view at the pressures from 0.3 to 0.8 GPa. (e) Pressure changes in the relative intensities. The intensity of S0 (1) mode obtained at each pressure was used for normalization of the intensity for S0 (J) mode, respectively.

Figure 3

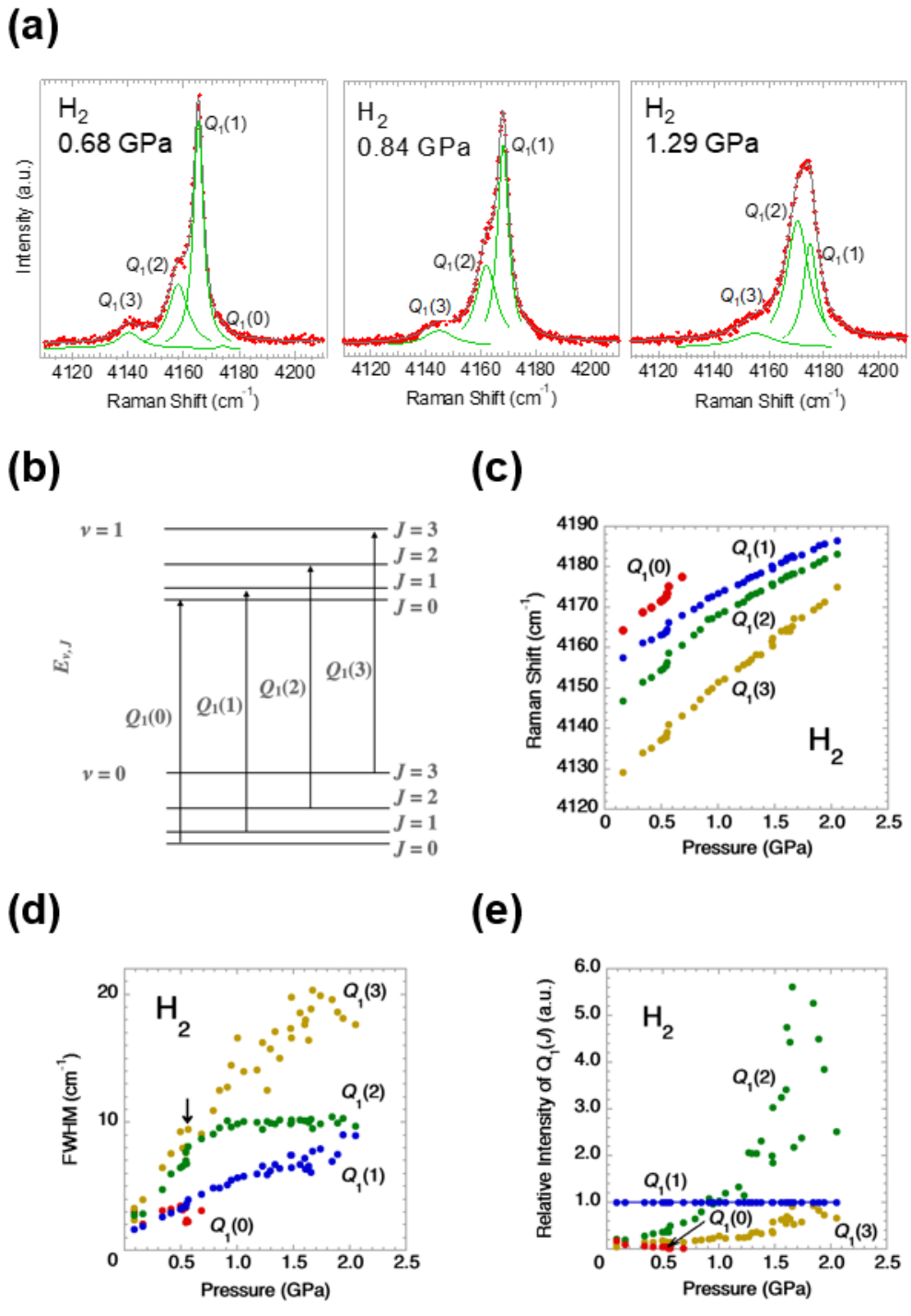

Figure 3

Pressure dependence of Raman shift, FWHM and relative intensity of Q1(J) band, obtained from H2. (a) Results of peak-separations of Q1(J) bands of H2, measured at 0.68, 0.84, and 1.29 GPa, at room

temperature, respectively. The red circles are experimental values, and green and gray curves are Lorentz curves used for the curve fitting and spectral approximate curves obtained by the curve fitting, respectively. The values of coefficients of determination R2 are obtained to be approximately 0.997 for these spectra, which mean good agreement with the experimental data. (b) Scheme of vibration transitions in Q branches having the selection rules of $\Delta\upsilon = +1$ and $\Delta J = 0$ on the Stokes line. (c) Pressure dependences of Raman shifts. (d) Pressure dependences of FWHMs. (e) Pressure changes in relative intensities. The intensity of Q1 (1) mode obtained at each pressure was used for normalization of the intensity for Q1 (J) mode, respectively.

Figure 4

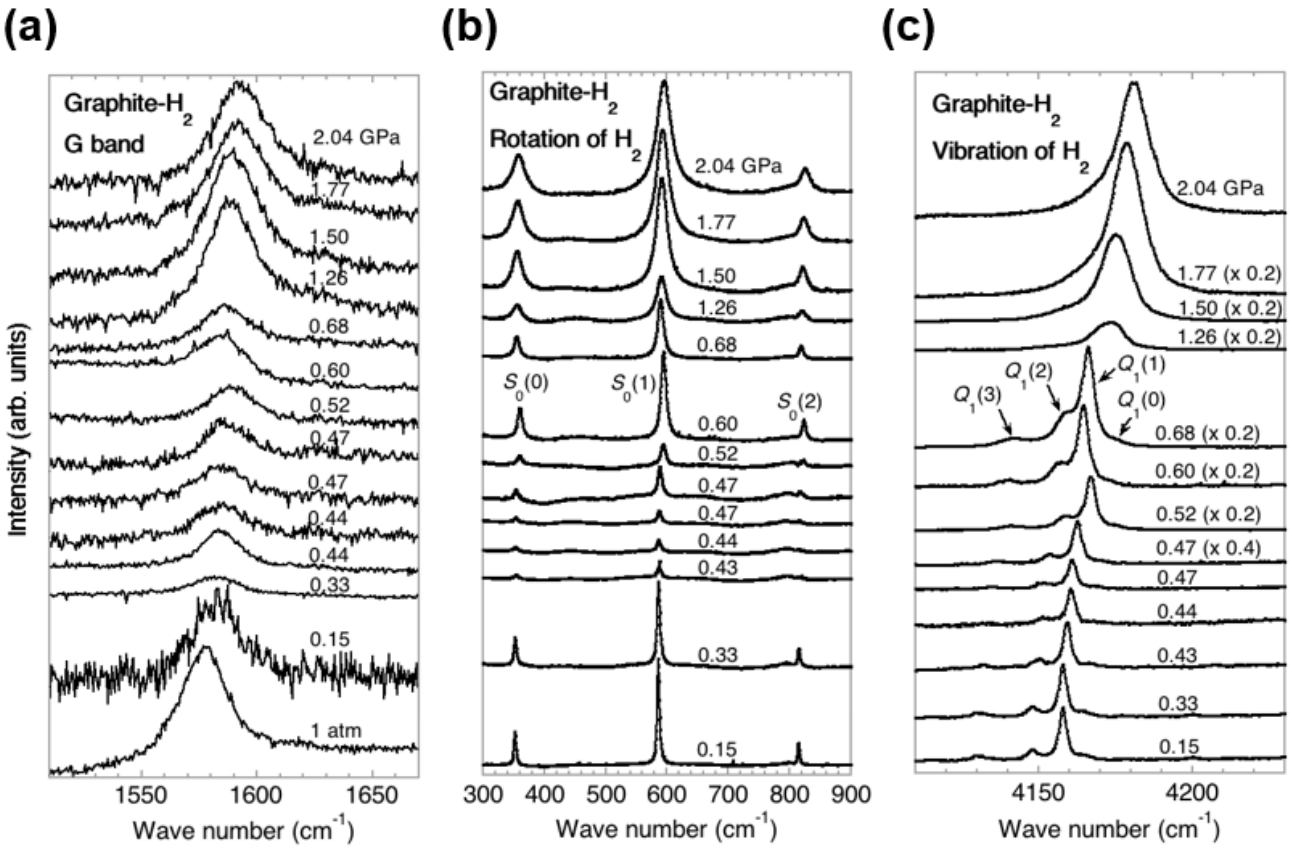

Figure 4

Superimposed display of Raman spectra of Graphite-H2 mixture under pressure up to 2.04 GPa at room temperature. (a) E2g mode from graphite (G-band). (b) Rotation mode S0 (J) from H2. (c) Vibration-rotation mode Q1(J) from H2. These spectra were measured by focusing on the surface of graphite through the diamond anvil. The G-band of graphite observed at 1 atm was also observed in order to compare with the spectra obtained from graphite-H2. The intensities of Q1 (J) mode obtained at 0.47 to

1.77 GPa were very strong, which were compressed in 20 to 40% of the originals to display the spectra compactly as shown in c.

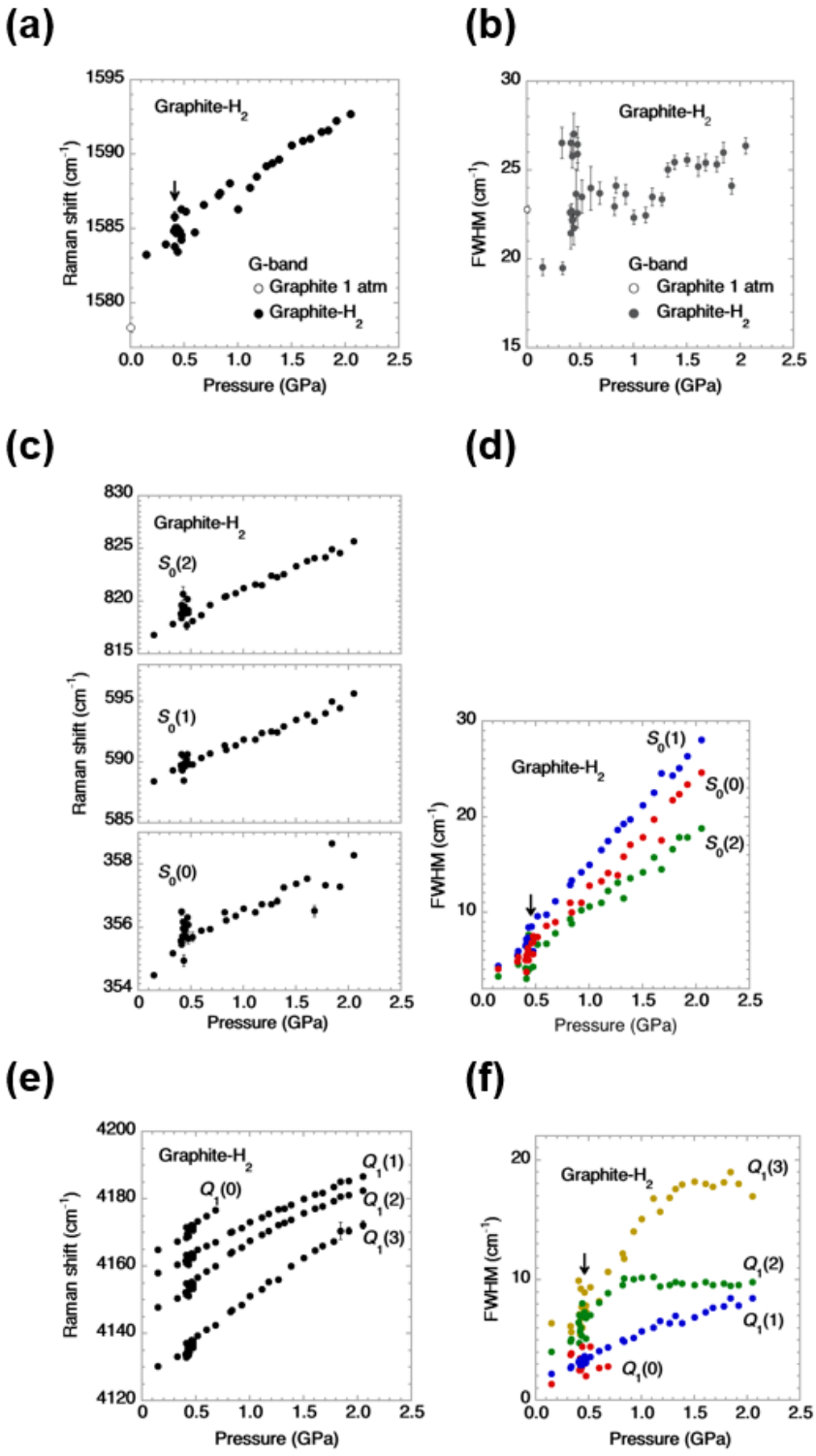

Figure 5

Pressure dependence of Raman shift and FWHM of G-band, S0(J) band and Q1(J) band, obtained from graphite-H2 mixture. (a) Raman shift of G-band of graphite. (b) FWHM of G-band of graphite. (c) Raman

shifts of S0 (J) bands of H2. (d) FWHMs of S0 (J) bands of H2. (e) Raman shifts of Q1(J) bands of H2. (f) FWHMs of Q1(J) bands of H2.

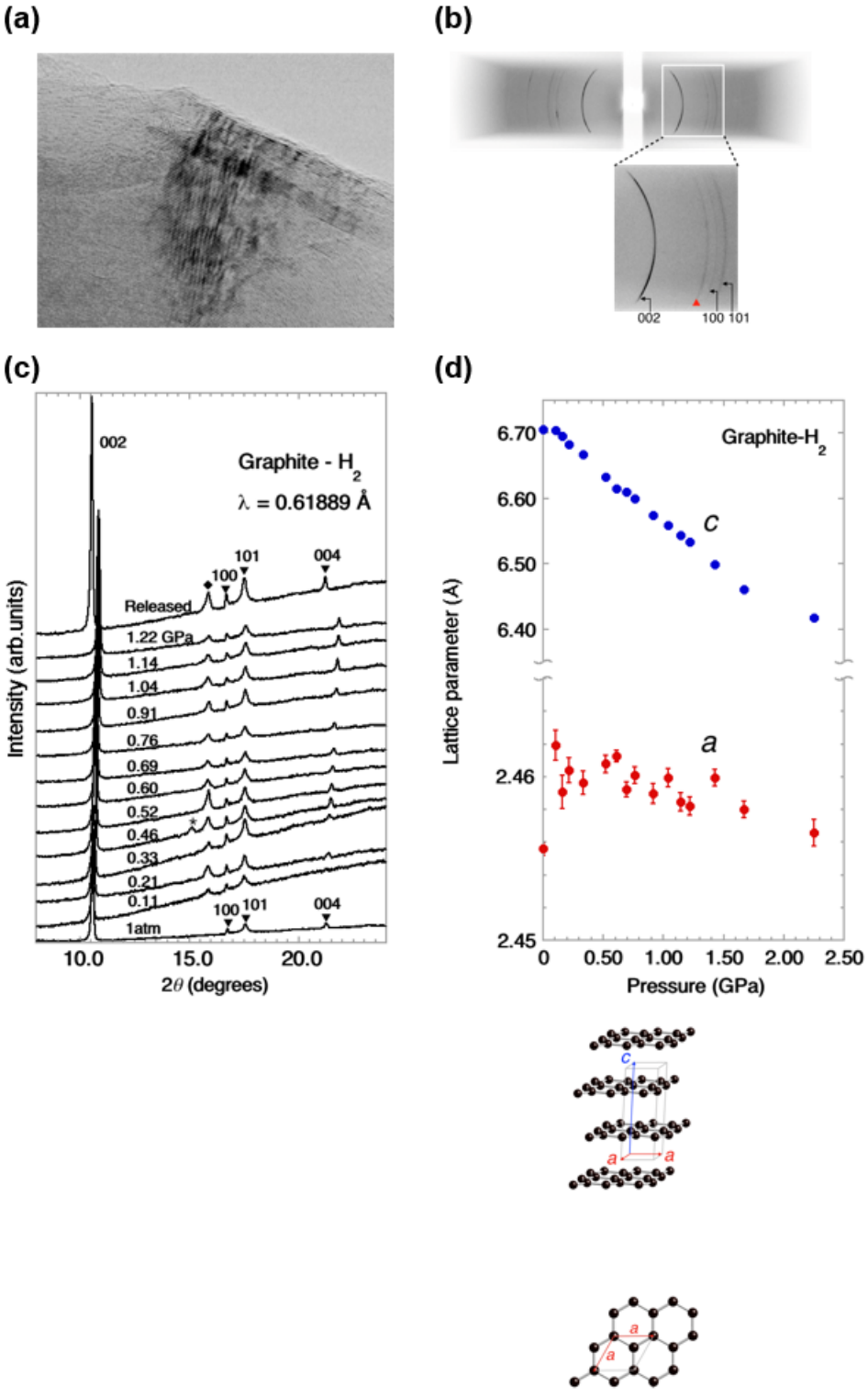

Figure 6

Structural feature of graphite and graphite-H2 mixture. (a) High resolution TEM image of graphite structure in MCMBs used as the sample. (b) Debye-Scherrer rings of graphite-H2 mixture pressurized at 0.11 GPa at room temperature. An unknown reflection marked with a solid triangle, was observed

between the 002 and 100 reflections from graphite. (c) XRD diffraction patterns of graphite before and after loading the pressure of H2 gas. The peaks marked with solid rhombuses and an asterisk indicate unknown reflections, respectively. (d) Pressure dependences of lattice parameters a and c of graphite-H2 mixture. We also showed the lattice parameters of graphite measured before pressurizing with H2.